Dalton Transactions

Accepted Manuscript

This article can be cited before page numbers have been issued, to do this please use: H. Zhang, D. Hedman, P. feng, G. Han and F. Akhtar, *Dalton Trans.*, 2019, DOI: 10.1039/C8DT04555K.

ROYAL SOCIETY OF CHEMISTRY

rsc.li/dalton

View Article Online
DOI: 10.1039/C8DT04555K

Journal Name

COMMUNICATION

High-entropy $B_4(HfMo_2TaTi)C$ and SiC ceramic composite

Hanzhu Zhang,[a] Daniel Hedman,[a] Peizhong Feng,[b] Gang Han[c] and Farid Akhtar*[a]

Received 00th January 20xx,
Accepted 00th January 20xx

DOI: 10.1039/x0xx00000x

www.rsc.org/

A multicomponent composite of refractory carbides, B_4C, HfC, Mo_2C, TaC, TiC and SiC, of a rhombohedral, face-centered cubic (FCC) and hexagonal crystal structures is reported to form a single phase $B_4(HfMo_2TaTi)C$ ceramic with SiC. The independent diffusion of the metal and nonmetal atoms led to a unique hexagonal lattice structure of the $B_4(HfMo_2TaTi)C$ ceramic with alternating layers of metal atoms and C/B atoms. In addition, the classical differences in the crystal structures and lattice parameters among the utilized carbides were overcome. Electron microscopy, X-ray diffraction and calculations using density-functional theory (DFT) confirmed the formation of a single phase $B_4(HfMo_2TaTi)C$ ceramic with a hexagonal close-packed (HCP) crystal structure. The DFT based crystal structure prediction suggest that the metal atoms of Hf, Mo, Ta and Ti are distributed on the (0001) plane in the HCP lattice, while the carbon/boron atoms form hexagonal 2D grids on the (0002) plane in the HCP unit cell. The nanoindentation of the high-entropy phase showed hardness values of 35 GPa compared to the theoretical hardness value estimated based on the rule of mixtures (23 GPa). The higher hardness was contributed by the solid solution strengthing effect in the multicomponent hexagonal structure. The addition of SiC as the secondary phase in the sintered material tailored the microstructure of the composite and offered oxidation resistance to the high-entropy ceramic composite at high temperatures.

Introduction

Ultrahigh temperature ceramics (UHTCs) like Zr_2B,[1, 2] HfB_2[3] and TaC[4, 5] with high thermal stability and remarkable mechanical properties, including high hardness, high mechanical strength and good wear resistance, can tolerate extreme working environments involving elevated temperatures and high loadings. These ceramics have been widely studied for high temperature applications in the form of monolithic ceramics and composites.[6-8] In terms of UHTC composites, silicon carbide has been incorporated to process UHTCs to tailor the microstructure and enhance the high temperature oxidation resistance.[9-13] Inspired by the concept of high-entropy alloys (HEAs), scientific efforts have been devoted to a new branch of UHTCs incorporating high-entropy ceramics (HECs). Developed from multicomponent ceramic compounds such as metallic oxides, nitrides or carbides, HECs show the possibility of forming single-phase solid solution, in both bulk and film forms.[14-16] The single-phase HECs display superior mechanical properties compared to conventional ceramic materials, due to severe lattice distortion and sluggish diffusion effect, which make them suitable for applications requiring high mechanical performance and phase stability at elevated temperatures.[17-19] The first crystalline HECs with a single-phase face-centered cubic (FCC) crystal structure were fabricated from metallic oxides by Rost, C.M. et al. in 2015.[20] Later, Joshua Gilda et al. sintered high-entropy diboride with a hexagonal close packed (HCP) crystal structure, which showed improved mechanical properties over individual borides.[14] Notably, the phase formation rules in HECs systems, i.e., thermodynamics and geometry criteria, are followed while designing HECs. In the recent HECs studies from Rost C.M.,[20] Joshua Gilda[14] and Elinor Castle,[21] the focus was on using one certain ceramic system, either metal oxide, boride or carbide. It is considered that as the starting materials in a HECs system, ceramic compounds (preferably metallic ceramic compounds with only one nonmetallic element) have the least geometrical difference in their lattice structures and can lead to a single-phase solid solution.

B_4C is well-known to have a high melting point, high strength and relatively low thermal expansion and conductivity. An HECs composite containing B_4C and other UHTCs such as HfC, Mo_2C, TaC, TiC and SiC can theoretically benefit by gaining reinforcement effects from all the constituents.[22-25] However, HECs combining both boride and carbide systems have not been attempted because of the large differences in their

[a] Division of Materials Science, Luleå University of Technology, 971 87 Luleå, Sweden
[b] School of Materials Science and Engineering, China University of Mining and Technology, 221116, Xuzhou, China
[c] School of Materials Science and Engineering, University of Science and Technology Beijing, 100083, Beijing, China

physical and crystallographic properties, including, for example, that the density of HfC is 12.2 g/cm^3 while the density of B_4C is low as 2.52 g/cm^3. Moreover, the aforementioned ceramic system shows vast differences in its crystal structures (FCC, HCP and rhombohedral), which makes forming the high-entropy phase from these constituents challenging.

In this research, a new high-entropy ceramic composite containing the UHTC constituents HfC, Mo_2C, TaC, TiC, B_4C and SiC whiskers (SiC_w) was designed and in situ synthesized and consolidated by pulsed current processing (PCP). The single-phase HECs were achieved in an unconventional high-entropy system containing four metal atoms (Hf, Mo, Ta, and Ti) and two nonmetallic atoms (C and B). The high-entropy phase was assessed using electron microscopy and X-ray diffraction (XRD). The distribution of atoms in the HCP high-entropy crystal structure was investigated by experimental XRD and evolutionary crystal structure predictions using density-functional theory (DFT). The nanoindentation hardness, oxidation behaviour and wear resistance properties of the SiC-HECs composite were investigated and, showed remarkable improvement of the mechanical properties and oxidation resistance.

Results and discussion

The microstructure of the high-entropy ceramic (HEC) composite in Fig. 1 shows that the PCP sintered HEC composite consists of two phases. According to the corresponding energy-dispersive X-ray spectroscopy (EDS) compositional mapping, the bright phase has uniform distribution of the Hf, Mo, Ta and Ti metal atoms, and the dark phase is rich in Si and C in the composite. The bright high-density phase in the microstructure refers to the high-entropy ceramic $B_4(HfMo_2TaTi)C$ phase, and the low-density dark phase represents SiC, according to the sensitivity of atomic number by backscattered electron detector.[26] The volume fraction of these phases was estimated to be 3:1 (bright: dark phase) by the "point counting" method (ASTM E562-08).[27] It can be seen that the SiC whiskers lost their rod-like shape and coalesced, while the high-entropy phase is displayed as "connected islands" with a grain size of 5~10 µm in the microstructure. A similar microstructure of the composite and the morphology change of the SiC_w reinforcement at high sintering temperature (>1600 °C) have also been observed in other UHTC-SiC_w composite.[28-30] The addition of SiC_w in ceramic composite inhibited the grain growth of the HEC phase, which can be beneficial to the mechanical properties of the composite by grain-boundary strengthening mechanism.[28, 31] The average composition ratio of metal atoms in the HEC phase was investigated by compositional mapping analysis on the high-entropy phase at ten different locations. It was found that the high-entropy solid solution consisted of equal-atomic ratio of the four metallic elements, which was consistent with the mixing ratio of the starting precursors excluding SiC. As EDS lacks the accuracy for the detection of light elements,[32] the present of B and C in the HEC phase was investigated by the wavelength dispersive X-ray spectroscopy (WDS). In Fig. 1b, the WDS spectrum recorded from the high-entropy phase confirms that the HEC phase consists of all four metal elements (Hf, Mo, Ta and Ti) and the nonmetallic elements (C and B). Therefore, we conclude that the precursor carbides (B_4C, HfC, Mo_2C, TaC and TiC) have formed single-phase solid solution, and SiC_w as the secondary phase is uniformly distributed in the microstructure.

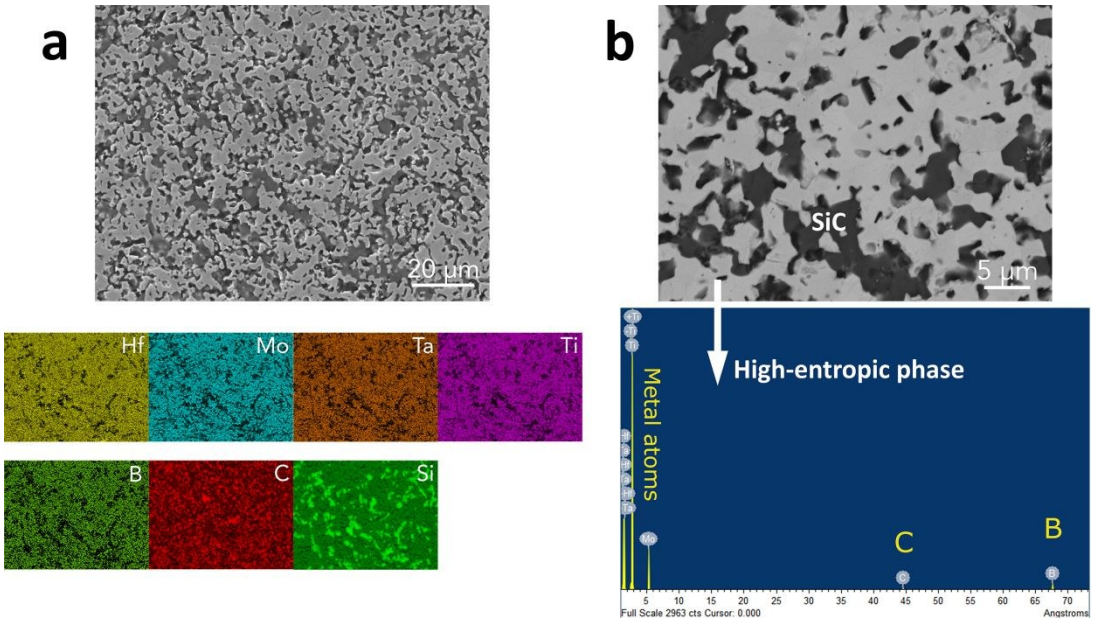

Fig. 1 The microstructure of the PCPed HECs composite show the presence of two different phases. Both (a) EDS compositional mapping and (b) WDS analysis show that the bright high-entropy ceramic phase contains Hf, Mo, Ta, Ti, C and B.

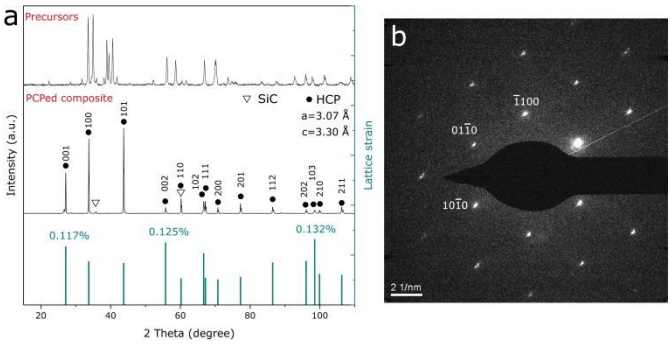

Fig. 2 The phase identification of the HEC composite. The XRD diffratograms of high-entropy ceramic composite in (a) shows the phase evolution before/after PCP and the calculated lattice strain in the individual lattice planes, the crystal structure was shown in the SAD pattern (b) taken from the high-entropy ceramic phase in the PCPed composite.

The X-ray diffraction (XRD) data in Fig. 2a show the phase evolution from precursors with various crystal structures to a single-crystal structure after sintering. The HEC phase exhibits a hexagonal close-packed (HCP) crystal structure, which is confirmed by the selected area diffraction (SAD) pattern taken from the high-entropy phase (Fig. 2b). The lattice parameters of the obtained high-entropy phase were identified from the XRD pattern as a = 0.307 nm and c = 0.330 nm. The lattice planes of the HCP structure identified in Fig. 2a are denoted by considering the primitive hexagonal unit cell. The lattice strain for individual reflection planes of the HCP structure was calculated by the Wilson equation[33] included in XRD analysis software Highscore Plus after subtracting Kα2 radiation for the analysis. The current high-entropy ceramic phase shows an average lattice strain of 0.083%, with the highest strain on the (001), (002) and (103) plane, which is lower than the reported lattice strain in a metallic high-entropy system (1-2%).[34, 35]

Compared with the precursor carbides, it can be seen that HEC has smaller lattice parameters but a similar cell volume (0.02693 nm^3) (Table 1). The refractory carbides from Group IV and Group V are well known for the mutual solubility. Among the metallic carbide precursors in this study, the system has the maximum mutual solubility when HfC, TaC or TiC act as the solvent carbide compared to Mo_2C being the solvent carbide.[36] In addition, Ta has the lowest metal vacancy formation energy in the carbide (3.5 eV) compared with Hf (9.3 eV) and Ti (8.6 eV),[21] thereby suggesting that the metal atoms diffuse into the TaC lattice rather than Ta diffusing into other carbide lattices. Another significant fact is that in carbide lattices, the diffusion of metal atoms is independent of that of carbon atoms.[21, 37] The self-diffusion rate of carbon has been reported to be several orders of magnitude faster than metal atoms, because carbon atoms jump to a tetrahedral hole before they migrate to the carbon vacancy whilst metal atoms only migrate to metal vacancies,[38] resulting in lower activation energy of carbon self-diffusion.[39] Therefore, we extrapolated that the whole-phase transformation process toward the HEC phase in the high-temperature ceramic composite includes two important parts. The first stage is the complex rearrangement of atoms with the FCC metal carbide TaC acting as the host lattice and, the elements Hf, Ti, Mo, C and B from other constituents migrating as guest atoms through the diffusion process. During the diffusion process, metal atoms and C/B atoms diffuse independently in their own sublattices (metal and nonmetal atoms) and form alternating layers in the lattice. Apart from the complex diffusion process, the host FCC lattice structure also experience a change in the stacking sequence, resulting in a high-entropy phase with Hf, Mo, Ta, Ti, B and C atoms presented in the HCP lattice. Such a phase transition from an FCC to HCP structure, which is induced by the pressure in high-entropy system, has been reported.[40]

In a traditional high-entropy alloy system, the atomic size difference (δ) between the solute and solvent atoms should be less than 15% in order to form substitutional solid solutions, and the crystal structure of elements is suggested to be the same according to the Hume-Rothery (H-R) rules.[41] Because of the existence of two different sublattices (metal and nonmetal atoms) and their independent diffusion behavior in current carbide system, H-R theory cannot define the phase selection rule. Based on the discussion of the complex diffusion process, the choice of metal atoms is considered to be the essential factor in the formation of high-entropy ceramic solid solution. We have determined the geometric factor $\delta_{a'}$ from four metal carbides HfC, Mo_2C, TaC and TiC.

Since metal atoms migrate only to the nearest metal vacancy on their original planes, suggesting that the migration of metal atoms occurs only at the close packed planes of (111) for FCC metal carbides and (0001) for Mo_2C (HCP), respectively. Thus the lattice length a' was determined based on their close packed planes. Since HfC, TaC and TiC have a rocksalt (NaCl) crystal structure that contains 8 atoms per cell, a' was calculated based on the reduced primitive cell by Equation (1), while a' for Mo_2C stays the same as its lattice parameter a.

Table 1 The calculation of lattice difference $\delta_{a'}$ in the HECs system

Component	Crystal structure	Niggli-reduced cell volume (nm^3)	Lattice parameters a (nm)	Lattice length at the close-packed plane a' (nm)	$\delta_{a'}$
HfC	FCC	0.02497	0.4640	0.3281	4.84%
TaC	FCC	0.02211	0.4442	0.3141	
TiC	FCC	0.02024	0.4315	0.3060	
Mo_2C	Hexagonal	0.03676	0.3000	0.3000	
B_4C	Rhombohedral	0.10950	0.5600		

View Article Online DOI: 10.1039/C9DT04555K

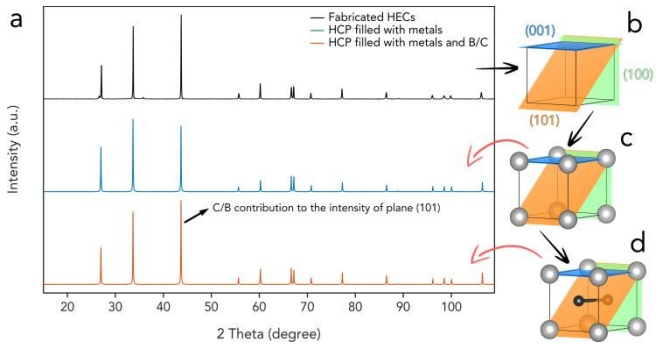

Fig. 3 Theoretical lattice structure for HEC phase derived from the experimental XRD results. (a) The experimental XRD pattern compared with simulated XRD patterns for the structures shown in (c) and (d). (b) the empty HCP HEC primitive unit cell showing the planes corresponding to the three highest diffraction peaks. (c) HEC lattice filled with metal atoms (gray) at (0,0,0) where all three planes intersect. (d) HEC lattice filled with both metal and nonmetal atoms (black) along the (101) plane at postions (1/3,2/3,1/2) and (2/3,1/3,1/2).

$$a' = \sqrt{2}a/2 \quad (1)$$

$$\delta_{a'} = \sqrt{\sum_{i=1}^{N} x_i \left[1 - {a'}_i / \left(\sum_{i=1}^{N} x_i a'_i\right)\right]^2} \quad (2)$$

where a', x and N represent the lattice length at the close packed plane, the molar fraction of the i^{th} component and the number of components, respectively. The crystal structure and lattice parameter were identified by experimentally collecting XRD diffractograms from all precursor materials. The calculated lattice size difference is $\delta_{a'} = 4.84\%$, which implies a high possibility of the formation of a single-phase solid solution among the four metal carbide compounds.

Based on the experimentally obtained XRD diffractogram, a theoretical prediction of the HEC crystal structure can be obtained. From the diffraction peaks in Fig. 2a we determine that the primitive Bravais lattice is hexagonal with lattice parameters of a, b = 0.307 nm and c = 0.330 nm. As the highest intensity peaks correspond to the (001), (101) and (101) lattice planes, atoms with the highest atomic scattering factor (the metal atoms) were placed at a point in the lattice where these planes intersect. As seen in Fig. 3b the intersection point of these planes is the origin (0,0,0). With only the metal atoms placed in the lattice (Fig. 3c), a simulated XRD pattern that closly matches the experimental one was obtained. However, it is clear from Fig. 3a that a lattice containing only metal atoms underestimates the intensity of the peak corresponding to the (101) plane.

The difference in the reflection intensity for plane (101) is due to the absence of carbon/boron in the simulated lattice. This finding implies that the fabricated high-entropy phase contains a carbon/boron hexagonal-shaped 2D grid in the (002) plane of the HCP lattice, which is consistent with the assumption of the independent diffusion of metal and carbon/boron atoms. Thus we extrapolate that the position of the nonmetal atoms in the lattice must lie on the (101) plane, in order to intensify the peak corresponding to this plane. The placement of the nonmetal atoms is thus determined to be at postions (x,y,z)=(1/3,2/3,1/2) and (2/3,1/3,1/2) in the lattice. With the lattice filled with both metal and nonmetal atoms at the determined postions (Fig. 3d), a simulated XRD diffractogram which matches experiemnts very well is obtained. This crystal structure is also similar to the one suggested by Joshua Gilda et al.[14] for their high-entropy diboride.

To verify the theoretical prediction for the HEC crystal structure, DFT based evolutionary crystal structure predictions were performed using XtalOpt[42] in combination with the Vienna ab initio simulation package (VASP).[43] Based on the composition of the precursors, the ratio of nonmetal atoms to metal atoms is 1.8. The crystal structure predictions were performed with 8 metal atoms ($Hf_2Mo_2Ta_2Ti_2$) and 16 non-metal atoms ($B_{16x}C_{16(1-x)}$). This composition corresponds to a 2x2x2 supercell of the theoretically predicted HEC crystal structure. The results show that the predicted lowest energy structures for x=1 and x=0.875 matches our theoretically predicted crystal structure (see the supplementary information).

For further investigations using DFT calculations, the HEC was modeled using special quasi-random structures (SQS). Since the HEC lacks long range ordering due to its high-entropy nature, large SQS are required.[44] SQS of sizes 2x2x2, 4x4x4 and 6x6x6 repetitions (supercells) of the theoretically predicted HEC crystal structure were created using the alloy theoretic automated toolkit (ATAT).[45] The SQS supercells were created with different boron content x = 1.0, 0.875, 0.75, 0.625, 0.5, 0.375, 0.25, 0.125 and 0.0 (see supplementary information). The simulated XRD diffractogram for the fully relaxed SQS structures (both lattice and atomic positions) with x=1 is shown in Fig. 4. A 4x4x4 or larger SQS supercell is required in order to achieve convergence with respect to lattice parameters and formation enthalpy at 0 K. The XRD patterns for the fully relaxed 4x4x4 and 6x6x6 supercells show excellent agreement with the experimentally obtained XRD pattern. DFT calculations determine lattice parameters of a, b=0.308 nm, c=0. 333 nm and a formation enthalpy H_f = -2.29 eV, meaning that the HEC has a lower formation enthalpy than the

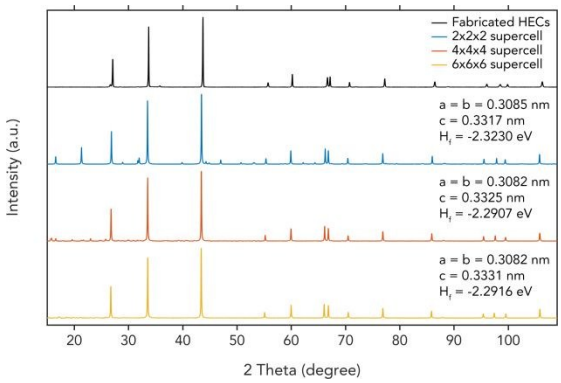

Fig. 4 Simulated XRD patterns for DFT optimized SQS of different sizes with x=1.0 compared with the experimentally obtained pattern. Inserts show the formation enthalpy at 0 K, H_f, and the lattice parameters, a, b, c for the fully DFT relaxed SQS (here the angles α, β, γ deviate less than 0.03 degrees from there theoretical values of 90, 90, 120 degrees)

precursors, HfC = -1.83 eV, Mo_2C = -0.28 eV, TaC = -1.16 eV, TiC

View Article Online
DOI: 10.1039/C8DT04555K

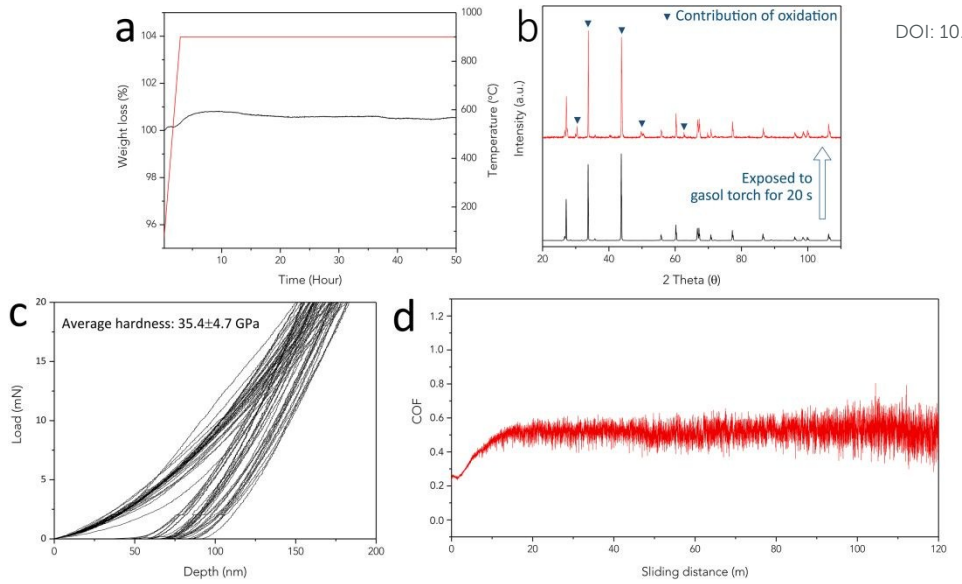

Fig. 5 The PCPed HEC composite shows remarkable properties. (a) Oxidation behaviour of the HEC composite is examined by exposing to air for 50 hours at 900 °C, (b) XRD patterns of the sample exposed to liquefied petroleum gas (LPG) for 20s in air, (c) Nanoindentation of PCPed HECs shows the average hardness values (35.4 GPa) of HEC phase, (d) The wear resistance shows the COF of sintered HECs bulk material is approximately 0.5 at a load of 10N.

= -1.66 eV and B_4C = -0.449 eV as calculated using DFT (see supplementary information). The formation enthalpy for the HEC at 0 K is lower than the precursors and the increase of TΔS term at elevated temperature can further reduce the free energy, points to energetically favorable conditions for the formation of high-entropy ceramic solid solutions during the PCP. The effect of different boron content, x, was investigated using 2x2x2 and 4x4x4 SQS (see supplementary information). The combination of experimental and simulation results show that the high-entropy ceramic phase can be synthesized from ceramic compounds with FCC, HCP and rhombohedral crystal structures. Independent diffusion of metal and carbon/boron atoms led to the alternating hexagonal layers in the obtained HCP crystal structure.

Since the HECs composite is designed for high-temperature applications, the resistance to oxidation was investigated under both a moderate temperature (900 °C) for long time and high temperature (2000 °C) for short time. The HECs composite was heated and exposed in air for 50 hours at 900 °C. It can be seen from Fig. 5a that the change in HEC weight was negligible throughout the measurement, which shows the resistance to oxidation of the HECs composite. We correlate this to the formation of silica protection layer from silicon carbide on the sample surface, as was reported previously for ceramic composites containing SiC.[46, 47] The sample was exposed to liquefied petroleum gas (LPG) torch, which has a flame temperature of 2000 °C,[48] for 20 s. The XRD patterns of the HEC composite before and after the torch experiment (Fig. 5b) are normalized at 2θ=27.1 °. A slight increase in peak intensity at 2θ=33.7 ° and 43.7 °, as well as a few weakly pronounced additional diffraction peaks, was observed in the XRD pattern of the oxidized HECs composite. These XRD diffraction peaks correspond to metallic oxides, HfO_2 and TaO_2. The mass of the specimen shows no increase after being heated by LPG torch in air, thus suggesting the oxidation process was hindered, possibly because the oxidation only took place close to the specimen surface and led to negligible mass increase. No obvious cracks are observed on the HEC composite surface after oxidation test. Both measurement strongly suggest that the PCPed $B_4(HfMo_2TaTi)C$ composite has remarkable oxidation resistance and is desirable to serve at elevated temperature working environments.

The nanoindentation of the PCPed HECs composite was performed on selected rectangular areas on the sample surface, showing a hardness of 35.4 GPa (Fig. 5c) and a Young's modulus of 472.4 GPa for the high-entropy phase. According to the rule of mixtures calculated from the hardness values of monolithic carbides, the theoretical hardness of the high-entropy phase is 23.2 GPa, which is 48% lower than the experimental result. The improvement of the mechanical performance over conventional carbide materials could be attributed to the solid solution hardening mechanism.[21] The wear resistance test was performed under a load of 10 N with a sliding distance of 120 m and a sliding speed of 100 rpm at room temperature. The initial increase in the coefficient of friction (COF) arises from the initial process of wear creation on the sample surface. The COF curve has a flat and consistent friction coefficient of 0.5 after the break-in procedure at the beginning.[49] The fluctuation of the curve is related to the lack of flatness on sample surface. No material transfer was observed on the microstructure of the wear ball or the evaluated composite surface.

Conclusions

Six different carbides with various crystal structures were mixed and sintered using pulsed current processing (PCP). The composite contains a high-entropy ceramic (HEC) phase $B_4(HfMo_2TaTi)C$ and coalesced SiC_w as the second phase in the microstructure. From the experimental XRD result a hexagonal

close-packed (HCP) crystal structure was suggested. The HCP crystal structure was confirmed by DFT based crystal structure searches, and is suggested to have a layered structure with alternating metal and carbon/boron layers as a result of the independent diffusion of metal and nonmetal atoms. The formation enthalpy of the HEC solid solution at 0 K is lower than that of the precursors, pointing to energetically favorable conditions for the formation of high-entropy ceramic solid solutions during the PCP process. The HEC phase $B_4(HfMo_2TaTi)C$ shows a high nanohardness (35.4 GPa), which is 48% higher than the theoretical value. The remarkable improvement in the mechanical performance is attributed to the solid solution strengthening mechanism. The high-temperature HEC composite also shows a low and consistent frictional coefficient. Moreover, the addition of SiC_w contributed to the excellent oxidation resistance of the sintered HEC composite.

Conflicts of interest

There are no conflicts to declare.

Acknowledgments

This work was supported by the Swedish Foundation for Strategic Research (SSF) for Infrastructure Fellowship (grant no. RIF14–0083), the National Natural Science Foundation of China (grant no. 51574241) and the bilateral project of NSFC-STINT (grant no. 51611130064). The authors would like to acknowledge the computational resources and knowhow provided by the Swedish National Infrastructure for Computing (project SNIC 2018/3-111) at High Performance Computing Center North (HPC2N).

References

1. S. S. Hwang, A. L. Vasiliev and N. P. Padture, *Materials Science and Engineering: A*, 2007, **464**, 216-224.
2. G. J. Zhang, Z. Y. Deng, N. Kondo, J. F. Yang and T. Ohji, *Journal of the American Ceramic Society*, 2000, **83**, 2330-2332.
3. M. Gasch, D. Ellerby, E. Irby, S. Beckman, M. Gusman and S. Johnson, *Journal of Materials Science*, 2004, **39**, 5925-5937.
4. E. Sani, L. Mercatelli, D. Fontani, J.-L. Sans and D. Sciti, *Journal of Renewable and Sustainable Energy*, 2011, **3**, 063107.
5. J. X. Liu, Y. M. Kan and G. J. Zhang, *Journal of the American Ceramic Society*, 2010, **93**, 370-373.
6. H.-T. Liu, J. Zou, D.-W. Ni, W.-W. Wu, Y.-M. Kan and G.-J. Zhang, *Scripta Materialia*, 2011, **65**, 37-40.
7. B. Nayebi, M. S. Asl, M. G. Kakroudi, I. Farahbakhsh and M. Shokouhimehr, *Ceramics International*, 2016, **42**, 17009-17015.
8. W. Fahrenholtz, G. Hilmas, A. L. Chamberlain and J. W. Zimmermann, *Journal of materials science*, 2004, **39**, 5951-5957.
9. N. P. Bansal, *Handbook of ceramic composites*, Springer Science & Business Media, 2006.
10. D. Liu, Y. Gao, J. Liu, K. Li, F. Liu, Y. Wang and L. An, *Journal of the European Ceramic Society*, 2016, **36**, 2051-2055.
11. P. F. Becher and G. C. Wei, *Journal of the American Ceramic Society*, 1984, **67**.
12. W. Gibbs, J. Petrovic and R. Honnell, 2009.
13. A. L. Chamberlain, W. G. Fahrenholtz, G. E. Hilmas and D. T. Ellerby, *Journal of the American Ceramic Society*, 2004, **87**, 1170-1172.
14. J. Gild, Y. Zhang, T. Harrington, S. Jiang, T. Hu, M. C. Quinn, W. M. Mellor, N. Zhou, K. Vecchio and J. Luo, *Scientific reports*, 2016, **6**.
15. W.-J. Shen, M.-H. Tsai, Y.-S. Chang and J.-W. Yeh, *Thin Solid Films*, 2012, **520**, 6183-6188.
16. Q.-W. Xing, S.-Q. Xia, X.-H. Yan and Y. Zhang, *Journal of Materials Research*, 2018, **33**, 3347-3354.
17. Y. Zhang, T. T. Zuo, Z. Tang, M. C. Gao, K. A. Dahmen, P. K. Liaw and Z. P. Lu, *Progress in Materials Science*, 2014, **61**, 1-93.
18. B. S. Murty, J.-W. Yeh and S. Ranganathan, *High-entropy alloys*, Butterworth-Heinemann, 2014.
19. J. W. Yeh, S. K. Chen, S. J. Lin, J. Y. Gan, T. S. Chin, T. T. Shun, C. H. Tsau and S. Y. Chang, *Advanced Engineering Materials*, 2004, **6**, 299-303.
20. C. M. Rost, E. Sachet, T. Borman, A. Moballegh, E. C. Dickey, D. Hou, J. L. Jones, S. Curtarolo and J.-P. Maria, *Nature communications*, 2015, **6**.
21. E. Castle, T. Csanádi, S. Grasso, J. Dusza and M. Reece, *Scientific Reports*, 2018, **8**, 8609.
22. D. Jianxin and S. Junlong, *Ceramics International*, 2009, **35**, 771-778.
23. T. Wang, C. Ni and P. Karandikar, in *Characterization of Minerals, Metals, and Materials 2016*, Springer, 2016, pp. 279-286.
24. C. Hwang, Q. Yang, S. Xiang, V. Domnich, A. U. Khan, K. Y. Xie, K. J. Hemker and R. A. Haber, *Journal of the European Ceramic Society*, 2018.
25. J.-L. Innocent, D. Portehault, G. Gouget, S. Maruyama, I. Ohkubo and T. Mori, *Materials for Renewable and Sustainable Energy*, 2017, **6**, 6.
26. J. I. Goldstein, D. E. Newbury, J. R. Michael, N. W. Ritchie, J. H. J. Scott and D. C. Joy, *Scanning electron microscopy and X-ray microanalysis*, Springer, 2017.
27. A. Standard, *ASTM E562-08*, 2008.
28. S. Sugiyama, D. Kudo and H. Taimatsu, *Materials transactions*, 2008, **49**, 1644-1649.
29. K. Farhadi, A. Sabahi Namini, M. Shahedi Asl, A. Mohammadzadeh and M. Ghassemi Kakroudi, *International Journal of Refractory Metals and Hard Materials*, 2016, **61**, 84-90.
30. C. Musa, R. Orrù, D. Sciti, L. Silvestroni and G. Cao, *Journal of the European Ceramic Society*, 2013, **33**, 603-614.
31. F. D. Gac and J. J. Petrovic, *Journal of the American Ceramic Society*, 1985, **68**.
32. B. K. Agarwal, *X-ray spectroscopy: an introduction*, Springer, 2013.
33. A. Wilson, *Journal*, 1949.
34. S. G. Ma and Y. Zhang, *Materials Science and Engineering: A*, 2012, **532**, 480-486.

View Article Online
DOI: 10.1039/C8DT04555K

35. S. Varalakshmi, M. Kamaraj and B. S. Murty, *Materials Science and Engineering: A*, 2010, **527**, 1027-1030.
36. H. O. Pierson, *Handbook of refractory carbides and nitrides: properties, characteristics, processing and applications*, William Andrew, 1996.
37. S. Ghaffari, M. Faghihi-Sani, F. Golestani-Fard and M. Nojabayy, *International Journal of Refractory Metals and Hard Materials*, 2013, **41**, 180-184.
38. J. Tobin, L. Adelsberg, L. Cadoff and W. Brizes, *Carbon diffusion in the group IVB and VB transition element monocarbides*, Westinghouse Electric Corp., Pittsburgh, Pa.(USA). Astronuclear Lab., 1965.
39. G. E. J. M. S. Hollox and Engineering, 1968, **3**, 121-137.
40. F. Zhang, S. Zhao, K. Jin, H. Bei, D. Popov, C. Park, J. C. Neuefeind, W. J. Weber and Y. Zhang, *Applied Physics Letters*, 2017, **110**, 011902.
41. W. Hume-Rothery, *McGraw-Hill, New York, 1967) p*, 1967, **3**.
42. D. C. Lonie and E. Zurek, *Computer Physics Communications*, 2011, **182**, 2305-2306.
43. G. Kresse and J. Furthmüller, *Physical Review B*, 1996, **54**, 11169-11186.
44. M. C. Gao, J.-W. Yeh, P. K. Liaw and Y. Zhang, *High-Entropy Alloys*, Springer, 2016.
45. A. van de Walle, P. Tiwary, M. de Jong, D. L. Olmsted, M. Asta, A. Dick, D. Shin, Y. Wang, L. Q. Chen and Z. K. Liu, *Calphad*, 2013, **42**, 13-18.
46. I. N. Godovannaya and O. I. Popova, in *Chemical Properties and Analysis of Refractory Compounds / Khimicheskie Svoistva I Metody Analiza Tugoplavkikh Soedinenii / Химические Свойства И Методы Анализа Тугоплавких Соединений*, ed. G. V. Samsonov, Springer US, Boston, MA, 1972, DOI: 10.1007/978-1-4615-8555-8_7, pp. 33-35.
47. K. Upadhya, J. Yang and W. Hoffman, *Am. Ceram. Soc. Bull*, 1997, **76**, 51-56.
48. D. Carinhana Jr, L. G. Barreta, C. J. Rocha, A. M. d. Santos and C. A. Bertran, *Journal of the Brazilian Chemical Society*, 2008, **19**, 1326-1335.
49. T. Chapman, D. Niesz, R. Fox and T. Fawcett, *Wear*, 1999, **236**, 81-87.